Green Chemistry

Accepted Manuscript

ROYAL SOCIETY OF CHEMISTRY

www.rsc.org/greenchem

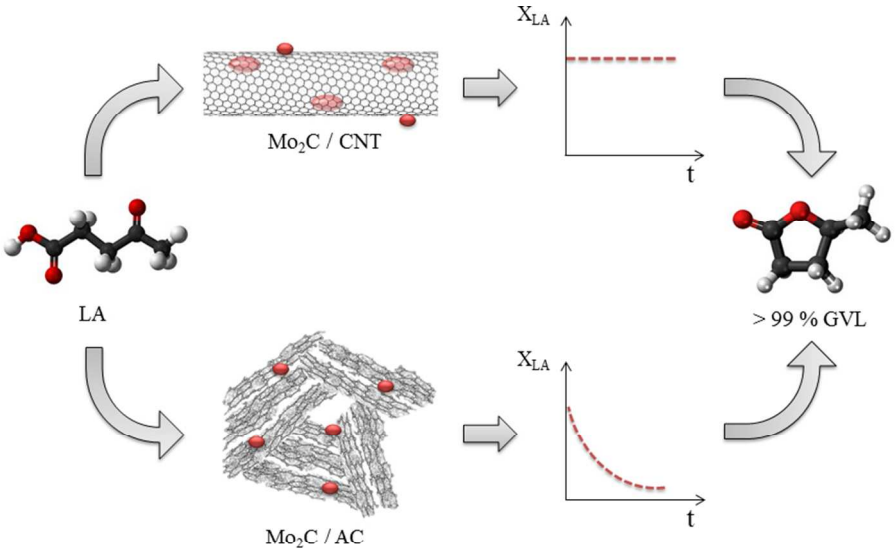

254x190mm (96 x 96 DPI)

Molybdenum carbide nanoparticles within carbon nanotubes as superior catalyst for γ-valerolactone production via levulinic acid hydrogenation

Estevão F. Mai[a], Marta A. Machado[a], Thomas E. Davies[b], Jose A. Lopez-Sanchez[b], Victor Teixeira da Silva[a,*]

[a] *Universidade Federal do Rio de Janeiro/COPPE/Chemical Engineering Program/NUCAT, P.O. Box 68502, Rio de Janeiro, RJ 21945-970, Brazil.*

[b] *Stephenson Institute for Renewable Energy, Chemistry Department, University of Liverpool, L69 7ZD, Liverpool, UK.*

Abstract: We report here for the first time that supported molybdenum carbide is an efficient catalyst to selectively convert levulinic acid into γ-valerolactone in aqueous phase. We have observed that the support plays a fundamental role over the activity and stability of molybdenum carbide that is stable when supported in carbon nanotubes but undergoes deactivation when supported on activated carbon. Particularly, when the carbide nanoparticles are positioned within the carbon nanotubes, conversions and selectivity values higher than 99 and 90 %, respectively, were observed at 30 bar of H_2 and 200 °C using a continuous-flow trickle-bed reactor. In a basis of per active site, these values are similar to those obtained for a ruthenium catalyst evaluated at the same conditions.

The use of waste biomass for the production of biofuels and high value-added chemicals is a key point towards the development of a sustainable economy. Indeed, biomass is the only renewable and sustainable source of organic molecules. In order to cope with the increasing demands in energy of the industrial and transport sectors, extensive research has been dedicated to improving the technologies which are able to transform biomass into value-added bio-derived compounds in a sustainable way. [1-2]

The conversion of residual biomass into platform molecules has attracted a great deal of attention because these platform molecules can be converted into an enormous variety of high value-added organic compounds. [2-5] In particular, the production of γ-valerolactone (GVL) via the selective hydrogenation of levulinic acid (LA) is arousing much scientific interest because of its applicability in several industrial sectors and the possibility of generating many valuable chemicals from it. [6-8] For instance, GVL can be used as a green solvent, a gasoline blender (can be mixed in any proportion to gasoline), [9] and as a diesel precursor (alkanes and alkenes can be produced through subsequent catalytic reactions). [2, 4]

Recent studies have shown that catalysts based on noble metals are the most effective in the catalytic hydrogenation of levulinic acid presenting an economic challenge that requires the development of new heterogeneous catalysts. Wright and Palkovits recently reviewed the literature [10] and concluded that ruthenium

based materials display better activity when compared to other active catalysts based on noble metals such as palladium, [11-12] iridium [13] or gold. [14-15] For instance, Tukacs et al. [16] compared three different catalysts in the hydrogenation of LA (10 % Pd/C, 5 % Ru/C and Raney-Ni) in a continuous-flow reactor and found the Ru-based catalyst achieved the highest conversion (82.9 %) at 100 bar and 100 °C. Similarly, Upare et al. [17] observed that a 5 % Ru/C catalyst exhibited higher activity (100 %) and selectivity to GVL (> 99%) when compared to Pd/C and 5 % Pt/C catalysts. However it is noteworthy that the work of Upare et al. [17] was carried out at atmospheric pressure, in gas phase using a continuous-flow reactor at a temperature of 265 ^{o}C. Under such conditions and without any solvent the high conversion and selectivity values are not surprising. Despite the good activity and selectivity observed in the aforementioned reports, precious metals are scarce and there are growing concerns about future supply, availability and increasing price, in particular for metals such as Ru, Pd and Pt. Currently, the use of precious metals increases the final production costs thus making the large scale production of GVL uneconomical, [18] this also adds additional risk when a new process for the production of bio-derivatives is being evaluated.

In this communication, we report supported molybdenum carbide to be a low cost catalyst for the hydrogenation of levulinic acid to γ – valerolactone in a continuous-flow liquid-phase reactor (Scheme 1). This catalyst is as active and selective as those based on noble metals. The use of molybdenum carbide as a low cost alternative is based on its well-known and proven features such as mechanical strength, high electrical and thermal conductivity and, mainly, its comparable catalytic behaviour to precious metals. [19-20]

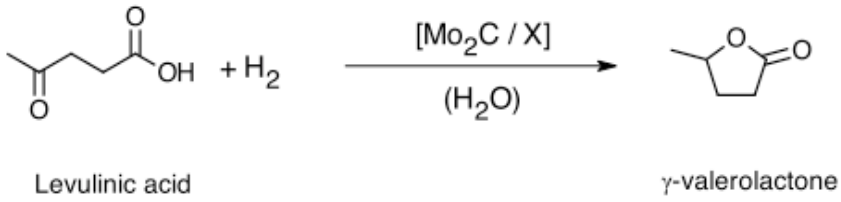

Scheme 1. Levulinic acid hydrogenation to γ-valerolactone in liquid phase using water as solvent.

Two different materials were used as supports for the molybdenum carbide active phase: activated carbon (AC) and carbon nanotubes (CNT). The carbide precursors were prepared by incipient wetness impregnation using an appropriate amount of aqueous solution of ammonium heptamolybdate to achieve 20 % (w/w) Mo_2C. The precursors were then submitted to temperature-programmed carburization (TPC) under a stream of 20 % (v/v) CH_4 / H_2 (100 mL min^{-1}) at 650 °C using a heating ramp of 2.5 °C min^{-1}. When the temperature reached 650 °C, the system was kept isothermal for 2 hours before being cooled down to room temperature [21]. Due to the pyrophoric nature of transition metal carbides, the samples were passivated under a mixture of 1 % (v/v) O_2 / N_2 (50 mL min^{-1}) over 12 hours before being exposed to the atmosphere. For comparison, a ruthenium catalysts supported on activated carbon (5 % (w/w)) was also synthesised. The ruthenium precursor was prepared by wetness impregnation using ruthenium (III) nitrosyl nitrate solution and temperature-programmed

reduction (TPR) was used to synthesize the catalyst using pure hydrogen (50 mL min^{-1}) – 200 °C / 2 hours and a heating ramp of 5 °C min^{-1}.

The crystalline phases present after synthesis where characterised by X-ray diffraction (XRD), shown in Figure 1, where asterisks represent the characteristic peaks of the corresponding support (activated carbon at 2θ = 24.3 °, 43.5 ° and 79.5 ° and carbon nanotubes 2θ = 23.5 º and 43.2 º). The dotted line depicts the main diffraction peak of β-Mo_2C located at 2θ = 39.4 º and attributed to the (1 0 1) plane in agreement with ICDD 35 – 0787. We found that the carbidic phase obtained after carburization of Mo_2C /CNT precursor using a CH_4/H_2 gas mixture was the β-Mo_2C crystalline structure This is shown by the presence of the main peak at 39.4 º in Figure 1b, and also by the presence of minor diffraction peaks at 2θ = 34.4 °, 37.9°, 52.1°, 61.5° and 75.5° (represented by the arrows in Fig. 1b) in the sample Mo_2C/CNT which are characteristic of the beta phase. These observations contrast with observations by Frank et al.[22] that indicated the preferential formation of an α – MoC_{1-x} phase instead of β-Mo_2C upon carburization of MoO_3/CNT using a CH_4/H_2 gas mixture. However, it must be noted that β-Mo_2C is the phase commonly obtained when bulk MoO_3 is used as starting material. [20]

The diffraction peaks corresponding to the beta Mo_2C are also partially visible for the AC supported catalyst, but are of lower intensity due to the high dispersion of the molybdenum carbide nanoparticles over the high specific surface area activated carbon; 678 m^2 g^{-1} as compared to 270 m^2 g^{-1} for the carbon nanotubes. Indeed, this hypothesis is supported by the transmission electron microscopy (TEM – Fig. 2a) analysis showing that while the average particle size for the particles supported on AC is 1.0 nm (Fig. 2b) with a narrow distribution (range from 0.5 to 3 nm), the particles supported on CNT are slightly bigger presenting a mean particle size of 3.3 nm and a narrow distribution (Fig. 3c).

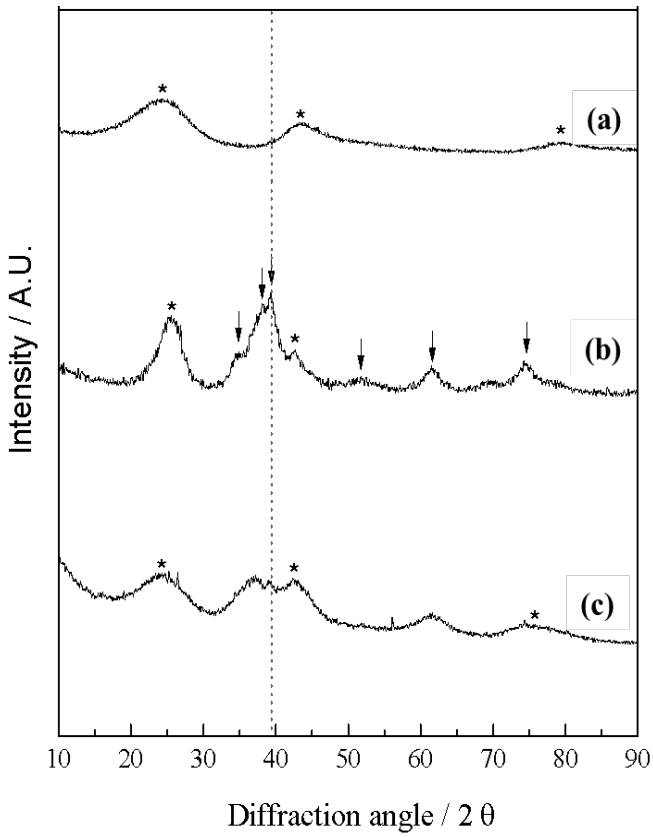

Figure 1. X – ray diffraction of 5 % Ru/AC (a), 20 % Mo_2C/CNT (b) and 20 % Mo_2C/AC (c). The asterisks show the characteristic diffraction peaks of the supports. The arrows show the diffraction peaks of the β-Mo_2C.

Similarly, we believe that the low ruthenium content (5 % (w/w)) together with the high surface area of the AC is the reason why ruthenium diffraction peaks could not detected (Fig. 1a).

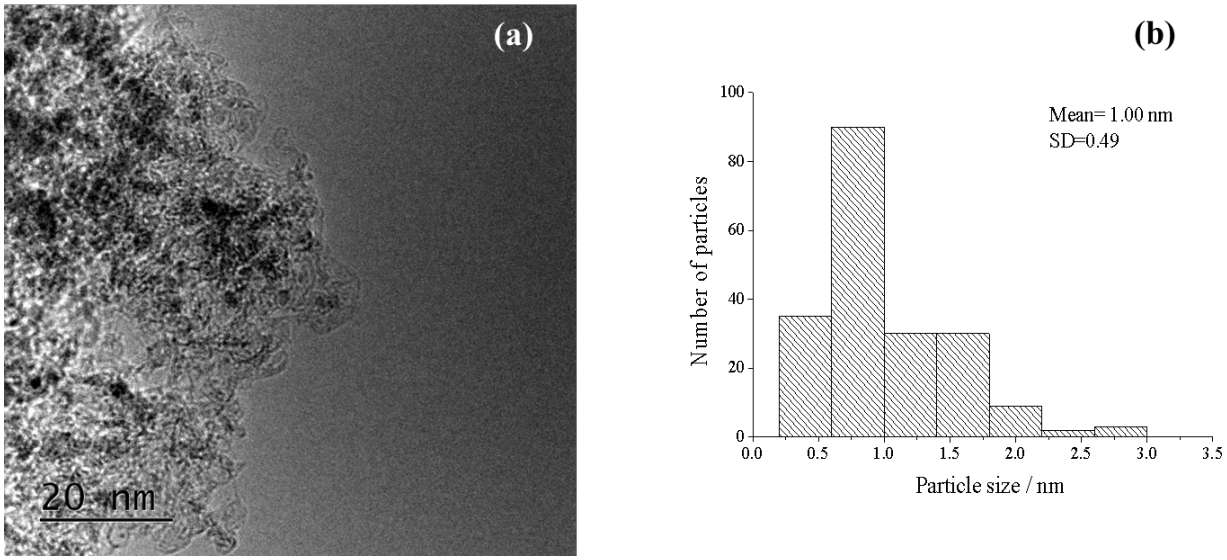

Figure 2. TEM micrograph of Mo_2C/AC at 250 kx (a) and its particle size distribution (b).

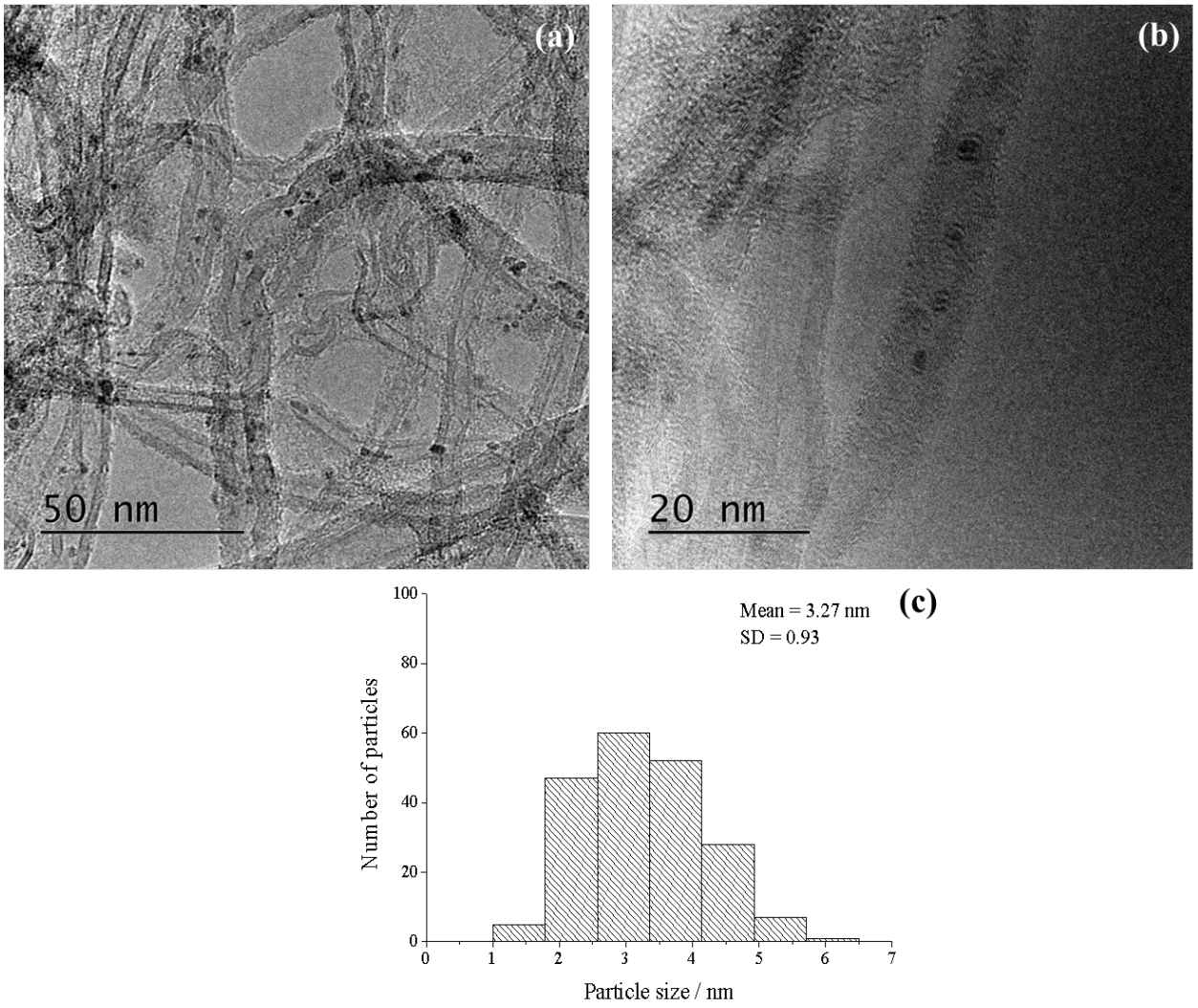

Figure 3. TEM micrographs of Mo_2C/CNT at 150 kx (a), 300 kx (b) magnifications and the particle size distribution (c).

When clusters of atoms are deposited onto supports they tend to ball up forming hemispherical particles.[23-24] Careful inspection of Figure 3 indicates that most of the Mo_2C particles are elongated thus suggesting that they are located inside the carbon nanotubes rather than on its outside walls. This is a clear example of how the support can affect the particle size, morphology and dispersion. On the other hand, Chen et al. [25] have shown that the covalent bonding between external Mo_2C nanoparticles and carbon nanotubes produces a charge transfer from molybdenum to carbon thus changing de d-band centre causing a dramatic change in activity. [26]

Taking this into account, the different catalytic performances of Mo_2C/CNT and Mo_2C/AC in the hydrogenation of levulinic acid to γ-valerolactone is shown in Fig. 4 can be explained. The reaction was carried out in an automatic continuous-flow trickle bed reactor (Microactivity, PID Eng&Tech, model MAPGLM3) where the performance of Mo_2C/AC and Mo_2C/CNT (Figure 4) was evaluated at 30 bar and three different temperatures (100, 150 and 200 °C) using a liquid space velocity (LHSV) of 3 h^{-1}. Prior to testing, blank experiments were done to investigate if the supports would present any activity. It was found that none of them displayed any significant activity (X_{LA} < 5 %).

As shown in Figure 4a, at 100 °C the LA conversion was low for Mo_2C/AC (X_{LA} ~ 8 %), while Mo_2C/CNT presented a higher value of conversion (X_{LA} ~ 16 % - Fig. 4b). The same trend was observed when the temperature was increased to 150 °C with Mo_2C/AC presenting a lower conversion (X_{LA} ~ 16 %) than Mo_2C/CNT (X_{LA} ~ 41 %). The difference in the conversion obtained for both catalysts at 100 and 150 ºC already indicates the influence exerted by the supports over the reaction where the utilization of carbon nanotubes contributes positively for a higher conversion of levulinic acid. This improvement becomes even clearer when the results at 200 ºC are analysed. As can be seen in Fig. 4a and Fig. 4b, despite having a high initial conversion at 200 ºC (approx. 95 %), the sample Mo_2C/AC showed considerable deactivation over the reaction time, whereas the catalyst Mo_2C/CNT kept its conversion steady and higher than 99 %.

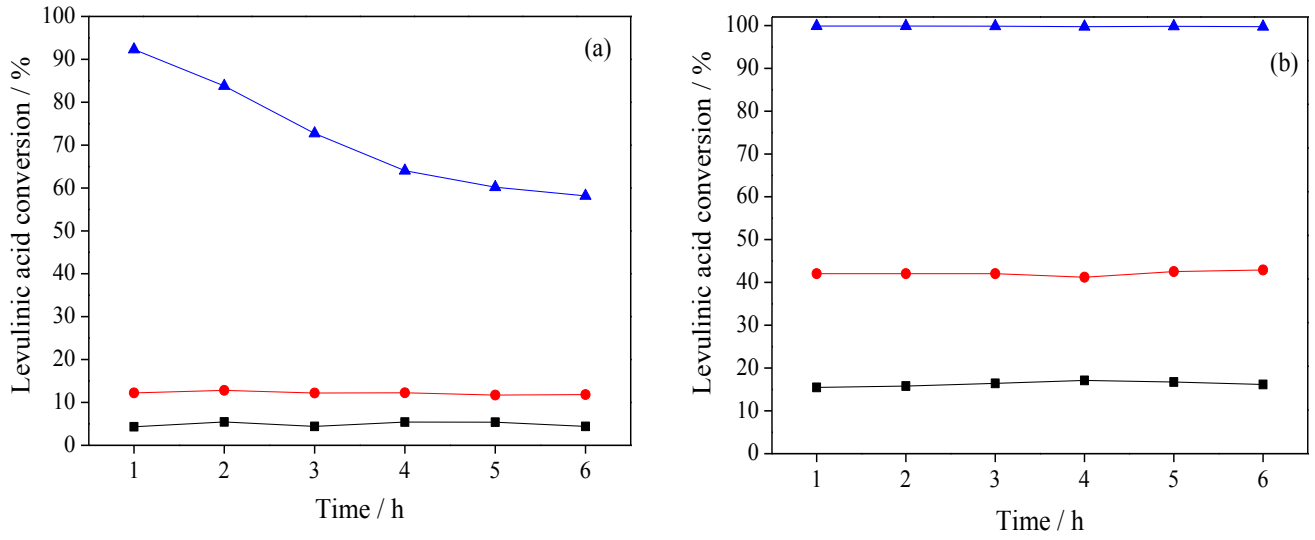

Figure 4. Levulinic acid conversion versus time over Mo_2C/AC (a) and Mo_2C/CNT (b) at 30 bar of H_2 and LSHV = $3h^{-1}$. Tests performed at 100 ºC (■), 150 ºC (●) and 200 ºC (▲).

Besides the excellent activity showed by the β-Mo_2C phase, it is noteworthy that, regardless the choice of the support, the values of selectivity to γ-valerolactone were always above 90 %. In the case of Mo_2C/CNT, the high selectivity and activity was kept over 24 for hours of reaction without any signs of deactivation or changes in selectivity.

The positioning of particles on the internal walls of nanotubes and the charge transfer effects have been used by many authors to create nanoreactors [27-29] with differentiated electronic properties that can improve the catalytic performance of supported metals in hydrogenation reactions. [30-32] The remarkable properties shown by metal particles either encapsulated by carbon nanotubes or located on the external walls are ascribed to the effect of electron confinement caused by the electron deficiency of the internal walls of the CNT or to charge transfer effects between the external particles and the CNT, respectively. In summary, the deformation of sp^2 hybridization in CNT walls causes the π-electron density to shift from concave inner surface to the convex surface of the external walls of CNT leading to an electron-deficient interior surface and an electron-enrich exterior surface [23 – 24]. Additionally, the observed stability could also either be a consequence of the encapsulation of the particles within the CNT where they are better protected against leaching or oxidation,

(two of the most probable causes for the deactivation) or due to change in the de d-band centre of the particles deposited on the external walls. The encapsulation effect has previously been observed for catalytic iron species, where the reducibility of the iron species and its resistance to oxidation was enhanced when inside the CNT as compared to species located on the external walls. [18, 33] We suggest that the additional stability observed for Mo_2C/CNT might also be due to this confinement effect that protects the nanoparticles from deactivation via oxidation, thus preserving the original phase.

In order to evaluate the potential of Mo_2C as an alternative replacement to noble metal based catalysts, we prepared and tested a 5 % (w/w) ruthenium catalyst on activated carbon of known high activity for levulinic acid hydrogenation. [2, 10, 34] The catalytic results on line at several temperatures are displayed in Figure 5.

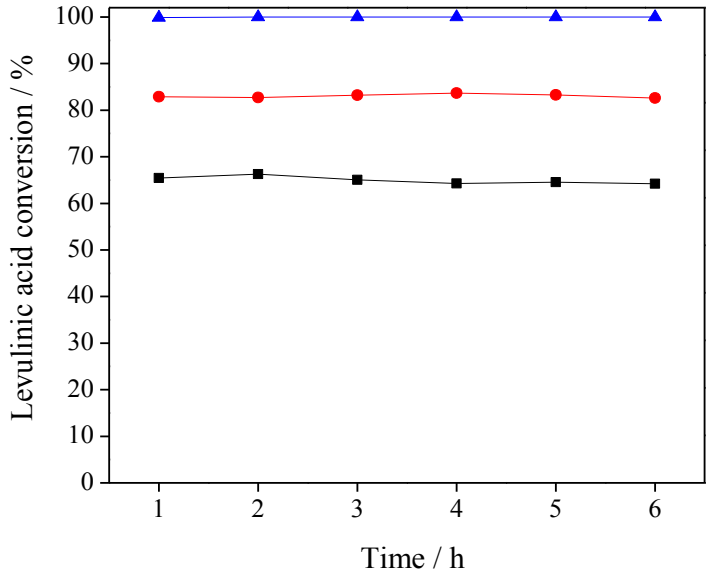

Figure 5 - Levulinic acid conversion versus time over 5 % Ru/AC at 30 bar of H_2 and LSHV = $3h^{-1}$. Tests performed at 100 ºC (■), 150 ºC (●) and 200 ºC (▲).

At 100 ºC the levulinic acid conversion was approximately 65 %, whereas at 150 and 200 ºC the conversion was 83 % and 100 %, respectively. This observation alone indicates that the ruthenium-based catalyst is more active than the Mo_2C-based catalysts. However, in order to properly contrast the specific activity of the Mo_2C phases with ruthenium, TOF values were calculated allowing for a quantitative correction based upon metal active sites. CO chemisorption studies, a well establish technique to quantify the number of active sites in transition metal carbides [35,36], were carried out and the values of turnover frequency (TOF) determined at 100 ºC and 150 ºC are presented in Table 1. The TOF values were calculated assuming a pseudo-first order reaction because the concentration of hydrogen was kept practically constant over the reaction time due to the high ratio between the liquid flow (levulinic acid aqueous solution) and gas flow, which was 1000.

Table 1. Turnover frequency values for 20 % Mo_2C/AC, 20 % Mo_2C/CNT and 5 % Ru/AC for the hydrogenation of LA to GVL at 30 bar of H_2 and different temperatures.

Sample	CO Chemisorption (μmol CO g_{cat}^{-1})	TOF (h^{-1})	
		100 ºC	150 ºC
20 % Mo_2C/AC	142	1.9	4.5
20 % Mo_2C/CNT	172	4.8	10.3
5 % Ru/AC	737	2.8	2.3

The TOF values presented in Table 1 clearly show that the molybdenum carbide is superior to the ruthenium catalysts for the LA hydrogenation to GVL. Mo_2C/AC and Ru/AC displayed similar turnover frequencies at both temperatures (2-4 h^{-1}). However, the Mo_2C/CNT catalyst displayed a notably higher TOF and higher selectivity to GVL than the ruthenium catalyst. Besides that, Mo_2C/CNT (90.3 %) has shown to be as selective as the 5% Ru/AC (88.3 %) towards GVL. Amongst the by-products detected by GC/MS 2-methyltetrahydrofuran, α-angelic lactone, pentanoic acid and 1,4-pentanediol were the ones identified as can be seen in the supplementary information. The observation of by-products formation for the 5% Ru/AC catalyst is in agreement with the work of Al-Shaal et al. [37] whom have performed the levulinic acid hydrogenation in a batch reactor at 130 °C and 12 bar using a 5% Ru/C catalyst and water as solvent. Under these conditions the authors obtained a conversion of levulinic acid of 99.5 % and a γ-valerolactone selectivity of 86.6 %, values similar to the ones obtained in our work. Despite the fact that was not possible to identify all of the by-products, GVL was the major product produced and the others represent less than 10 % of the total area on the chromatographic analysis.

It is well known that the transformation of levulinic acid to γ-valerolactone occurs through two major paths involving dehydration and hydrogenation reactions, as shown in Scheme 2. [10, 34, 37, 38]

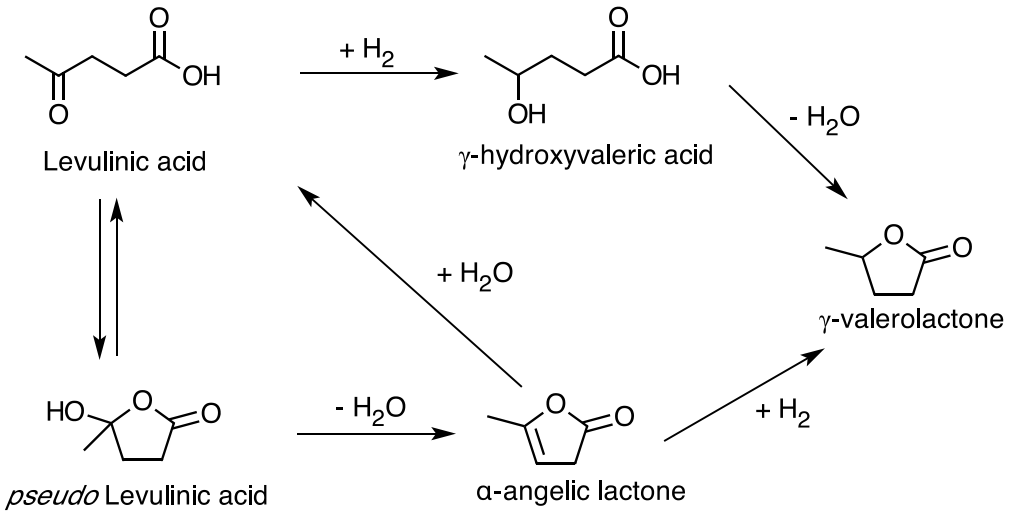

Scheme 2. Reaction pathways for γ-valerolactone formation.

The observation of small quantities of α-angelic lactone amongst the reaction products and the absence of γ-hydroxyvaleric acid could be an indicative that the levulinic acid hydrogenation on molybdenum carbide occurs through the α-angelic lactone path. However, the presence of pentanoic acid in the products could be due to dehydration/hydrogenation reactions of the γ-hydroxyvaleric acid, suggesting that the levulinic acid hydrogenation occurs through both pathways, as has already been reported in the literature. [34, 37, 38]

Although further investigation is required to fully understand the cause of the deactivation for the Mo_2C/AC, it has been shown for the first time that Mo_2C has a great potential to be used in the hydrogenation of levulinic acid to γ-valerolactone in aqueous phase using a continuous-flow trickle bed reactor. In particular, the use of carbon nanotubes led to a catalyst (Mo_2C/CNT) that not only has presented an excellent yield of GVL but also a higher activity per active site than that obtained for Ru/AC.

Conclusions

The selective production of γ-valerolactone through levulinic acid hydrogenation was successfully achieved at 30 bar of pressure using molybdenum carbide supported on activated carbon and on carbon nanotubes in a continuous reactor using water as solvent. We have discovered that supported molybdenum carbide is an efficient catalyst to selectively convert levulinic acid into γ-valerolactone in the aqueous phase. Particularly, when the carbide nanoparticles are positioned within the carbon nanotubes, conversions and selectivities above 90 % were observed at 30 bar of H_2 and 200 °C using a continuous-flow trickle-bed reactor. The choice of carbon support had a large effect on particle size, morphology and catalyst activity. When the Mo_2C was prepared on carbon nanotubes most of nanoparticles are encapsulated within the nanotubes and the Mo_2C phase displays a higher TOF than ruthenium supported on activated carbon. In view of the sustainability and price limitations that noble metals have, the application of Mo_2C for γ-valerolactone production represents an excellent example of a necessary shift to more sustainable catalysts for the upgrade of bio-derived chemicals.

Acknowledgments

The authors thank CNPq (Conselho Nacional de Desenvolvimento Cientifico e Tecnológico) for the financial support. Davies and Lopez-Sanchez thank the EPSRC for financial support (grant EP/K014773/1), the Science and Technology Facilities Council for the microscopy facilities at Harwell research campus and the Department for Business Skills and Innovation (Regional Growth Fund, MicroBioRefinary project).

Notes and references

X – Ray powder diffraction (XRD) analysis was carried out on a Panalytical diffractometer (model X`Pert Pro HTS) with copper radiation (Cu Kα = 1.5418 Å). The samples were scanned from 2θ = 10 º to 2θ = 90 º at a

speed of 1 º per minute. Transmission electron microscopy (TEM) analyses were performed in a JEOL JEM-2100 at 200 kV. The identification and quantification of the liquid products was done using a GC-MS (Agilent, model 7890 – 5975C) equipped with an automatic injector, mass selective detector and flame ionization detector (FID). For the analysis, a VF-Waxms (Polyethylene glycol, 30 m x 0.25 mm x 0.30 mm) capillary column was used with a temperature program of 80 to 250 ºC at a heating rate of 8 ºC min^{-1}. CO-pulsed chemisorption measurements were obtained by pulsing calibrated volumes of 20 % (v/v) CO/He gas mixture and following online the ion m/z = 28 with a mass spectrometer (Pfeiffer Vacuum, model D-35614 Asslar).

1 J. C. Serrano-Ruiz, A. Pineda, A. Balu, R. Luque, J. M. Campelo, A. A. Romero, J. M. Ramos-Fernández, *Catal. Today*, 2012, **195**, 162-168.

2 M. J. Climent, A. Corma, S. Iborra, *Green Chem*., 2014, **16**, 516-547.

3 J. S. Luterbacher, J. M. Rand, D. M. Alonso, J. Han, J. T. Youngquist, C. T. Maravelias, B. F. Pfleger, J. A. Dumesic, *Science*, 2014, **343**, 277-280.

4 D. R. Fernandes, A. S. Rocha, E. F. Mai, C. J. A. Mota, V. Teixeira da Silva, *Appl. Catal. A: Gen.*, 2012, **425 – 426**, 199-204.

5 J. J. Bozell, L. Moens, D. C. Elliott, Y. Wang, G. G. Neuenscwander, S. W. Fitzpatrick, R. J. Bilski, J. L. Jarnefel, *Resour. Conserv. Recy.*, 2000, **28**, 227-239.

6 D. M. Alonso, S. G. Wettstein, J. A. Dumesic, *Green Chem.*, 2013, **15**, 584-595.

7 J. M. Tukacs, D. Király, A. Strádi, G. Novodarszki, Z. Eke, G. Dibó, T. Kégl, L. T. Mika, *Green Chem.*, 2012, **14**, 2057-2065.

8 J. Lange, R. Price, P. M. Ayoub, J. Louis, L. Petrus, L. Clarke, H. Gosselink, *Angew. Chem. Int. Ed.*, 2010, **49**, 4479-4483.

9 I. T. Horváth, H. V. M. Fábos, L. Boda, L. T. Mika, *Green Chem.*, 2008, **10**, 238-242.

10 W. R. H. Wright, R. Palkovits, *ChemSusChem.*, 2012, **5**, 1657-1667.

11 K. Yan, T. Lafeur, G. Wu, J. Liao, C. Ceng, X. Xi, *Appl. Catal. A: Gen.*, 2013, **468**, 52-58.

12 K. Yan, C. Jarvis, T. Lafleur, Y. Quiao, X. Xi, *RSC Adv.*, 2013, **3**, 25865-25871.

13 W. Li, J. Xie, H. Lin, Q. Zhou, *Green Chem.*, 2012, **14**, 2388-2390.

14 X. Du, Q. Bi, Y. Liu, Y. Cao, K. Fan, *ChemSusChem.*, 2011, **4**, 1838-1843.

15 X. Du, L. He, S. Zhao, Y. Liu, Y. Cao, H. He, K. Fan, *Angew. Chem. Int. Ed.*, 2011, **50**, 7815-7819.

16 M. Tukacs, R. V. Jones, F. Darvas, G.Dibó, G. Lezsák, L. T. Mika, *RSC Adv.*, 2013, **3**, 16283-16287.

17 P. P. Upare, J. Lee, D.W. Hwang, S. B. Halligudi, Y. K. Hwang, J. Chang, *J. Ind. Eng. Chem.*, 2011, **17**, 287-292.

18 D. J. Braden, C. A.Hena, J. Heltzel, C. C. Maravelias, J. A. Dumesic, *Green Chem.*, 2011, **13**, 1755-1765.

19 L. Leclercq, K. Imura, S. Yoshida, T. Barbee, M. Boudart, *Stud. Surf. Sci. Catal.*, 1979, **3**, 627.

20 S. T. Oyama, *Catal. Today*, 1992, **15**, 179-200.

21 A. S. Rocha, A. B. Rocha, V. Teixeira da Silva, *Appl. Catal. A: Gen.*, 2010, **379**, 54-60.

22 B. Frank, K. Friedel, F. Girgsdies, X. Huang, R. Schlögl, A. Trunschke, *ChemCatChem.*, 2013, **5**, 2296-2305.

23 S. Schauermann, N. Nilius, S. Shaikhutdinov, H.-J. Freund, *Acc. Chem. Res.*, 2013, **46**, 1673-1681.

24 H.-J. Freund, N. Nilius, T. Rissec, S. Schauermanna, *Phys. Chem. Chem. Phys.*, 2014, **16**, 8148-8167.

25 W. F. Chen, C. H. Wang, K. Sasaki, N. Marinkovic, W. Xu, J. T. Muckerman, Y. Zhu, R. R. Adzic, *Energy Envirom. Sci.*, 2013, **6**, 943-951.

26 X. Bian, M. D. Scanlon, S. Wang, L. Liao, Y. Tang, B. Liu, H. H. Girault, *Chem. Sci.*, 2013, 4, 3232.

27 X. Pan, Z. Fan, W. Chen, Y. Ding, H. Luo, Z. Bao, *Nat. Mater.*, 2007, **6**, 507-511.

28 Q. Ma, D. Wang, M. Wu, T. Zhao, Y. Yoneyama, N. Tsubaki, *Fuel*, 2013, **108**, 430-438.

29 E. Castillejos, P. Debouttiere, L. Roiban, A. Solhy, V. Martinez, Y. Kihn, O. Ersen, K. Philippot, B. Chaudret, P. Sherp, *Angew. Chem. Int. Ed., 2009*, **48**, 2529-2533.

30 Z. Guan, S. Lu, C. Li, *J. Catal.*, 2014, **311**, 1-5.

31 H. Yang, S. Song, R. Rao, X. Wang, Q. Yu, A. Zhang, *J. Mol. Catal. A: Chem.*, 2010, **323**, 33-39.

32 W. Chen, Z. Fan, X. Pan, X. Bao, *J. Am. Chem. Soc.*, 2008, **130**, 9414-9419.

33 W. Chen, X. Pan, M. Willinger, D. S. Su, X. Bao, *J. Am. Chem. Soc.*, 2006, **128**, 3136-3137.

34 Z. Yan, L. Lin, S. Liu, *Energ. Fuels*, 2009, **23**, 3853-3858.

35 J. S. Lee, K. H. Lee, J. Y. Lee, J. Phys. Chem., 1992, **96**, 362-366.

36 M. Nagai, H. Tominaga, S. Omi, Langmuir, 2000, **16**, 10215-10220.

37 M. G. Al-Shaal, W. R. H. Wright, R. Palkovits, Green Chem., 2012, **14**, 1260-1263.

38 A. M. R. Galleti, G. Antonetti, V. De Luise, M. Martinelli, Green. Chem. **14**, 688-694.